JOURNAL OF MATERIALS SCIENCE 40 (2005) 1909–1915

The effect of Sn concentration on some physical properties of zinc oxide films prepared by ultrasonic spray pyrolysis

V. BILGIN, S. KOSE, F. ATAY, I. AKYUZ
Department of Physics, Osmangazi University, 26480 Eskisehir, Turkey

The effect of Sn concentration on zinc oxide (ZnO) film properties has been investigated by depositing films with various Sn concentrations in the solution (Sn/Sn + Zn ratio from 0 to 50 at%) at a substrate temperature of 350°C by ultrasonic spray pyrolysis (USP) technique. The deposited films were characterized for their electrical, structural, morphological and elemental properties using current-voltage and conductivity-temperature measurements, X-ray diffraction, scanning electron microscopy and energy dispersive X-ray spectroscopy. Electrical investigations showed that the resistivity of ZnO films decreases for lower Sn concentration (at 10%) and then increases for higher Sn concentration (at 30–50%). Also, depending on the increasing Sn concentration, energies of donor-like traps for ZnO films decreased and activation energy of donors for ZnO films increased. The XRD patterns showed that the as-deposited films have polycrystalline structure and the crystalline nature of the films was deteriorated with increasing Sn concentration and a shift to amorphous structure was seen. The effect of Sn concentration was to increase the surface roughening and change considerably the morphologies of ZnO films. The most homogenous surface was seen in ZnO films. EDS results showed that all elements in the starting solutions were in the solid films and Zn element is more dominant than Sn on the surfaces. After all investigations, it was determined that Sn incorporation dramatically modifies the properties of ZnO films. ZnO and ZnO:Sn (10 at%) films have a low resistivity and high transparency in the visible range and may be used as window material and antireflecting coating in solar cells while the other films may be used in gas sensors where high conductivity is unnecessary. © *2005 Springer Science + Business Media, Inc.*

1. Introduction

TCO (transparent conducting oxides) layers have been studied extensively because of a wide range of technical applications, e.g. as transparent electrodes in photovoltaic and display devices, sensors, etc. [1–3]. Among the conducting oxides, zinc oxide (ZnO) and tin oxide (SnO_2) films have been attracting interest since they have many important applications in solar cells, optoelectronic devices, liquid crystal displays, heat mirrors, thin film resistors and gas sensors [4–6]. These materials have high transparency in the visible and near infrared region of the electromagnetic spectrum and show n-type conductivity. The electrical conductivity of these films is mainly due to oxygen deficiency [7–9].

ZnO and SnO_2 films have been grown using several methods, such as chemical vapor deposition (CVD), spray pyrolysis, evaporation, sputtering, atomic layer epitaxy, pulsed laser deposition and sol-gel deposition [10–12]. Among these methods, spray pyrolysis is well suited for the preparation of these films because of its simple and inexpensive experimental arrangement, ease of adding various doping material, reproducibility, high growth rate and mass production capability for uniform large area coatings, which are desirable for industrial applications [13–15]. Ultrasonic spray pyrolysis (USP) is also known as a method to prepare submicrometer particles of metals and oxides. While spray pyrolysis is a standard technique, and hence not requires a detailed description, the ultrasonic enhancement is not, and should therefore be briefly explained: USP is very suitable for the fabrication of coatings because of the spherical shape and small size of the particles synthesised. It is an effective production technique which leads to short production time, homogeneous particle compositions and a one-step production method. The droplets generated by ultrasonic waves are not inert, so they can be transported by the carrier gases to a heated substrate where several reactions such as solvent evaporation and atomic rearrangement take place to form polycrystalline thin films. Compared with the particles prepared by solid state reactions, the particle size distribution is narrow, the purity of the products is high and it is easy to control the composition and morphology of powders [16, 17].

 © *2005 Springer Science + Business Media, Inc.*

TABLE I Amounts of spraying solutions used to deposit films and thickness of the produced films

Reactants	ZnO	ZnO:Sn (10 at%)	ZnO:Sn (30 at%)	ZnO:Sn (50 at%)
$Zn(CH_3COO)_2$ (cm^3)	200	180	140	100
$SnCl_2$ (cm^3)	–	20	60	100
Total (cm^3)	200	200	200	200
Thickness (μm)	3.25	4.50	4.83	4.13

This paper reports the effect of Sn concentration on the electrical, structural, morphological and elemental properties of ZnO films prepared by the USP technique.

2. Experimental procedure

ZnO and ZnO:Sn films, with Sn atom percentages of 10, 30 and 50%, were produced using an improved ultrasonic spray system described in previous works [18–21]. The spray solution was prepared by mixing the appropriate volumes of $Zn(CH_3COO)_2{\cdot}2H_2O$ (0.1 M) and $SnCl_2{\cdot}2H_2O$ (0.1 M) dissolved in deionized water. The solution was sprayed through ultrasonic nozzle onto microscope glass substrates (10×10 mm^2) using air as carrier gas with a pressure of 1.5 bar. 200 cm^3 of solution was used and sprayed during 40 min. The solution flow rate was kept at 5 cm^3 min^{-1} and controlled by a flowmeter. The distance between the nozzle and the substrate was maintained at 35 cm and the substrate temperature of 350°C was controlled within ±5°C by using an iron-constantan thermocouple. Electrical contacts were made by gold electrodes of thickness about 600 nm on the surfaces of the films using vacuum evaporation technique (Leybold Heraus 300 Univex). The thickness of the films were measured between 3.25 and 4.83 μm using the three-dimensional coating thickness gauge (Leitz PMM 12106). The experimental details of the mixed spraying solutions and the thickness of all the films are listed in Table I. The resistivities of the films were determined by the two-probe technique and the electrical conduction mechanisms of the films were investigated using Hewlett Packard 4140B pA Meter/DC voltage source. The conductivity-temperature measurements were made using a cryostat, a Fluke Voltage/Current Calibrator Model 382a and a Keithley 619 Electrometer. The structural properties of the films were studied using a X-ray diffractometer (XRD) with Cu K_α radiation (Rigaku model, $\lambda = 1.5405$ Å). The surface properties of all films were investigated using a CamScan scanning electron microscope (SEM). The elemental analyses of the films were performed by energy dispersive X-ray spectroscopy (EDS).

3. Results and discussion

3.1. Electrical characterization

To have information about the electrical properties of ZnO and ZnO:Sn films, electrical resistivities, conduction mechanisms and activation energies of all films are investigated.

3.1.1. Electrical conduction mechanisms and electrical resistivities

In order to investigate the electrical conduction mechanisms and to determine the resistivity of ZnO and ZnO:Sn films, current-voltage ($I - V$) characteristics of the films were obtained in the voltage range of 0.01–100 V in dark conditions. First of all, to see the existence and state of the traps in ZnO and ZnO:Sn films, the $I - V$ plots were drawn on log-log scale, and ohmic and space-charge-limited (SCL) current mechanisms were investigated. The $I - V$ plot of ZnO films is shown in Fig. 1a. In the voltage range of 0.01–50 V there is a almost linear increase in current with increasing voltage of the form $I \propto V^{0.90}$ where ohmic conduction is dominant. The increase is sharper in the high voltage region (50–100 V). This $I - V$ behavior suggests that ZnO films have deep trapped structures. The number of free carriers is higher than that of the injected ones in the ohmic region [22]. Then trap-filled-limited (TFL) conduction region comes where all of the traps are almost filled. In this region the current increases sharply with increasing voltage. The $I - V$ plot of ZnO:Sn (10 at%) films is shown in Fig. 1b. The current changed in the form of $I \sim V^{0.93}$ in the 0.01–100 V voltage range. The ohmic conduction is dominant in this region. The $I - V$ plot of ZnO:Sn (30 at%) films is shown in Fig. 1c. The current change is in the form $I \sim V^{0.95}$ in the 0.01–60 V voltage range. In the SCL conduction region where the current changes in the form of $I \sim V^{1.53}$, the number of injected carriers becomes higher, while the carriers are being trapped. Hence the current in SCL conduction region consists of both free and injected carriers [23]. The transition voltage between two regions is $V_{tr} = 60$ V. The $I - V$ plot of ZnO:Sn (50 at%) films is shown in Fig. 1d. The conduction mechanism for this film can be divided into two different regions, one as ohmic and the other TFL. These films have deep trapped structure. The current changes in the form $I \sim V^{1.03}$ and $I \sim V^{1.12}$ for the voltage range of 0.01–0.45 V and 1.4–60 V, respectively. In these regions, ohmic conduction is dominant and the number of free carriers is higher than that of the injected ones. Then a TFL region where all of the traps are almost filled takes place. The transition from the first ohmic region to the first TFL region and from the second ohmic region to the second TFL region $V_{TFL} = 0.45$ V and $V_{TFL} = 60$ V, respectively.

The resistivities of all films have been calculated in the ohmic regions of $I - V$ characteristics and given in Fig. 1, and are presented in Table II. The resistivity of the films is high at low Sn concentration $\rho \approx$ 1,1–1,3 10^2 Ωcm and increases with the concentration. This increase can be explained as follows: the concentration

TABLE II Resistivities (at room temperature) and activation energies of the ZnO and ZnO:Sn films

Material	ρ (Ωcm)	E_t (meV)	E_a (meV)
ZnO	1.36×10^2	366 (350–420 K)	5.24 (100–200 K)
ZnO:Sn (10 at%)	1.07×10^2	187 (310–380 K)	6.56 (100–170 K)
ZnO:Sn (30 at%)	3.83×10^2	91 (155–395 K)	51.90 (95–155 K)
ZnO:Sn (50 at%)	6.99×10^3	84 (235–395 K)	20.20 (90–140 K)

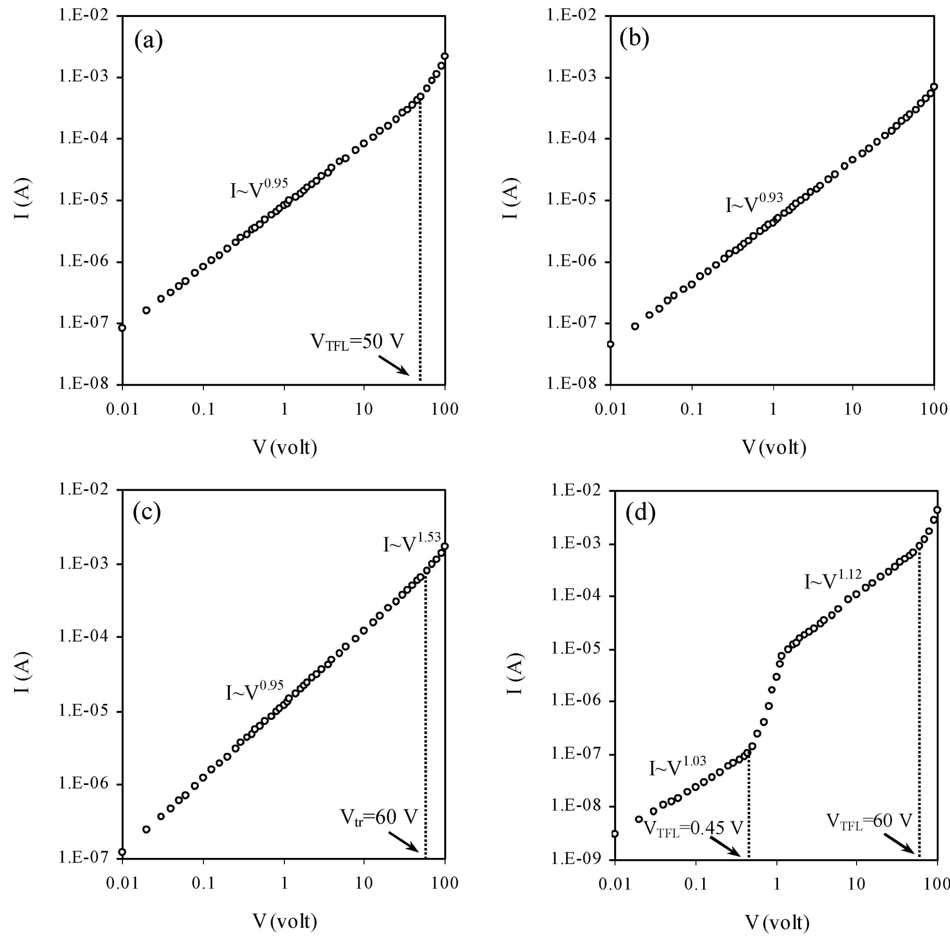

Figure 1 $I - V$ characteristics of (a) ZnO, (b) ZnO:Sn (10 at%), (c) ZnO:Sn (30 at%), (d) ZnO:Sn (50 at%) films.

of free charge carriers in ZnO increases by the Sn concentration, because Sn has two more valance electrons than Zn. We may consider that Sn substitutes the Zn atom or occupies the interstitial sites. In both cases, Sn acts as a donor. It was seen that the grain size decreases (Table III) with increasing Sn concentration. This causes the enhancing of grain boundary scattering. The source of the increase in conductivity (at10%) is the increase in carrier concentration. It subsequently decreases at further concentrations due to the grain boundary scattering. These results are in good agreement with the results reported by others [24–26].

To determine the electrical conductivity type of ZnO and ZnO:Sn films, hot-probe technique was used. It was seen that the films show an n-type conductivity, which is attributed to a deviation from stoichometry, due to the presence of oxygen vacancies, and interstitial atoms (Zn and/or Sn) in excess. Both oxygen vacancies and interstitial atoms act as donor impurities. This case is in good agreement with the results reported in literature [27].

TABLE III Crystalline phases, half peak widths, B, and grain size, t, of ZnO and ZnO:Sn films

Material	Crystalline phases	B × 10^{-3} (rad)	t (nm)
ZnO	ZnO	3.490	41.6
ZnO:Sn (10 at %)	ZnO + Zn_2SnO_4 + SnO_2	4.363	32.8
ZnO:Sn (30 at %)	ZnO + Zn_2SnO_4 + SnO_2	13.96	10.4
ZnO:Sn (50 at %)	ZnO + Zn_2SnO_4 + SnO_2	6.981	20.5

3.1.2. Activation energy measurements

The existence of the traps was observed when the results of the log I vs log V measurements on ZnO and ZnO:Sn films were investigated. To support this result and understand the general behavior of the conductivity in a large temperature range, the conductivity is plotted as a function of the temperature on a semi logarithmic scale ($\ln\sigma$ vs. $10^3/T$) in the temperature range of ~90–420 K. The shape of the plots indicates a semiconducting behavior of the materials.

At temperatures near room-temperature, deviations from a linear behavior in the conductivity temperature relationship became remarkable (Fig. 2). Thus, a double-valued activation energy was observed. One of them shows the activation energies of donors and the other one shows the energies of donor like traps. We can express this situation using this formula;

$$\sigma = \sigma_1 \exp(-E_a/kT) + \sigma_2 \exp(-E_t/kT), \quad (1)$$

where E_a is the activation energy of donors and E_t is the energy of donor-like traps, as mentioned above, k is the Boltzmann constant and σ_1 and σ_2 are the pre-exponential factors, respectively.

The activation energies of the films are listed in Table II. The donor levels are located at 5.24, 6.56, 51.9, 20.2 meV under the conduction band for ZnO, ZnO:Sn (10 at%), ZnO:Sn (30 at%), ZnO:Sn (50 at%) films, respectively. The values increase with Sn concentration, while that of the donor like traps energies decreased.

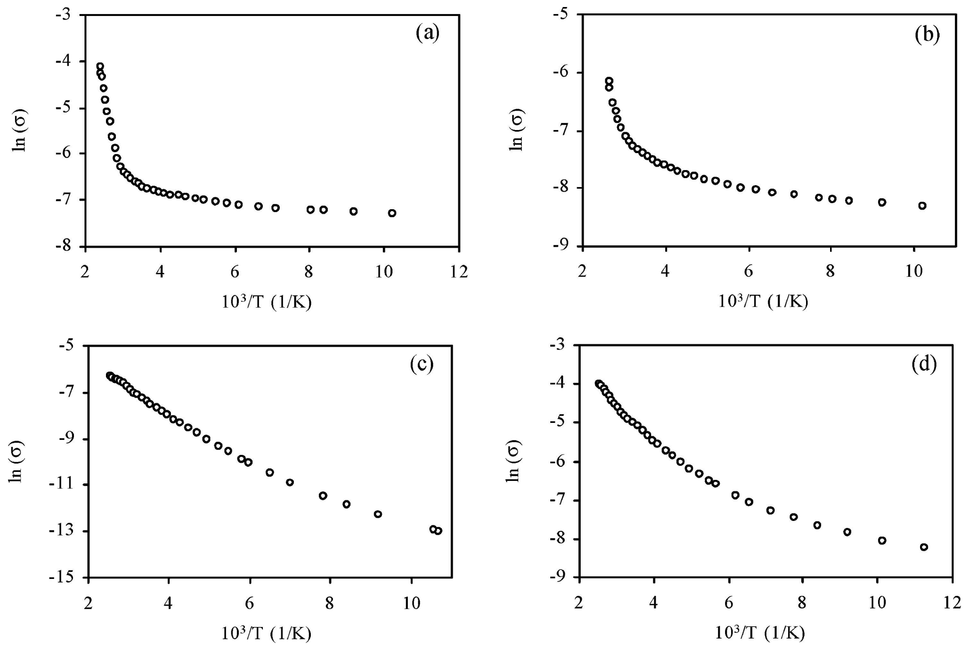

Figure 2 The $\ln(\sigma[\Omega \cdot \mathrm{cm}]^{-1}) \sim 10^3/\mathrm{T}(10^3/\mathrm{K})$ characteristics of (a) ZnO, (b) ZnO:Sn (10 at%), (c) ZnO:Sn (30 at%), (d) ZnO:Sn (50 at%) films.

3.2. Crystal structure

The structural properties of the films were investigated using XRD. The XRD patterns of all films are given in Fig. 3. The 2θ values were varied from 20 to 60°. All the films have a polycrystalline structure. The crystallinity of pure ZnO films is better than that of the other ones. In other words, the crystallinities of the ZnO films deteriorate with increasing Sn concentration. The XRD patterns of ZnO films indicate an hexagonal wurtzite structure. For ZnO films, the (002) peak predominates indicating a preferential growth. This means that the

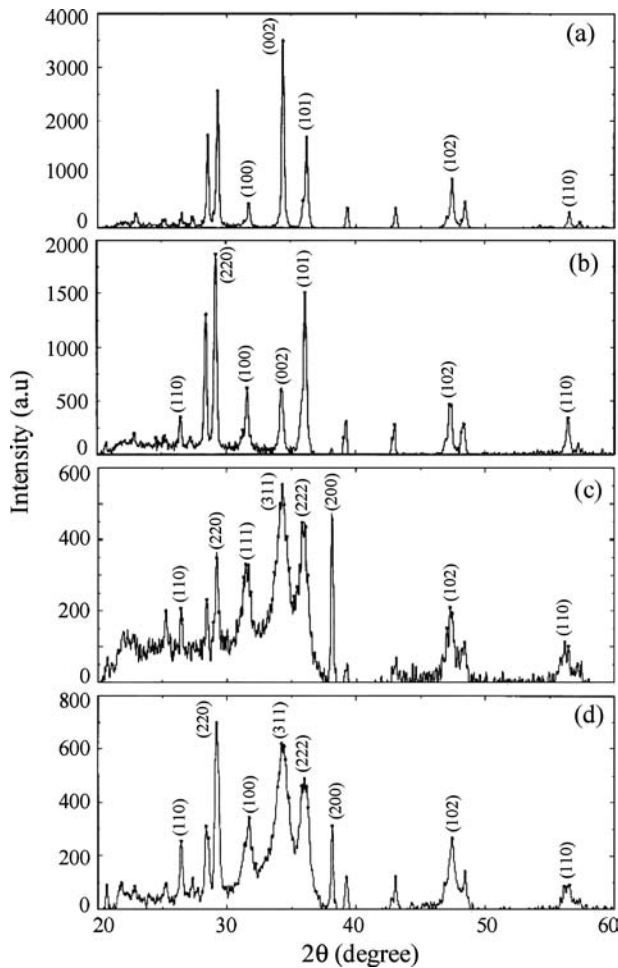

Figure 3 The XRD patterns of (a) ZnO, (b) ZnO:Sn (10 at%), (c) ZnO:Sn (30 at%), (d) ZnO:Sn (50 at%) films.

TABLE IV Lattice spacing (d), angle of diffraction (2θ), relative intensity of the peaks (I/I_0) and phases identified along with (hkl) planes of ZnO: Sn films

Material	2θ (deg)	d (Å)	I/I_{max} (%)	TC (hkl)	Identification with (hkl) values
ZnO	31.68	2.8220	13	0.745	(100) ZnO
	34.36	2.6078	100	5.734	(002) ZnO
	36.18	2.4807	48	2.752	(101) ZnO
	47.44	1.9148	26	1.491	(102) ZnO
	56.52	1.6269	8	0.459	(110) ZnO
ZnO:Sn	26.46	3.3657	19	0.773	(110) SnO_2
(10 at%)	29.22	3.0538	100	4.067	(220) Zn_2SnO_4
	31.62	2.8273	33	1.342	(100) ZnO
	34.24	2.6167	32	1.301	(002) ZnO
	36.10	2.4860	80	3.253	(101) ZnO
	47.26	1.9217	25	1.017	(102) ZnO
	56.42	1.6295	18	0.732	(110) ZnO
ZnO:Sn	26.42	3.3707	37	0.705	(110) SnO_2
(30 at%)	29.22	3.0538	63	1.201	(220) Zn_2SnO_4
	31.46	2.8413	60	1.144	(111) SnO_2
	34.28	2.6137	100	1.906	(311) Zn_2SnO_4
	35.82	2.5048	81	1.544	(222) Zn_2SnO_4
	38.16	2.3564	82	1.563	(200) SnO_2
	47.28	1.9210	38	0.724	(102) ZnO
	56.18	1.6359	20	0.381	(110) ZnO
ZnO:Sn	26.46	3.3657	37	0.949	(110) SnO_2
(50 at%)	29.20	3.0558	100	2.566	(220) Zn_2SnO_4
	31.72	2.8186	49	1.257	(100) ZnO
	34.22	2.6182	89	2.284	(311) Zn_2SnO_4
	36.00	2.4927	70	1.796	(222) Zn_2SnO_4
	38.14	2.3576	45	1.155	(200) SnO_2
	47.44	1.9148	38	0.975	(102) ZnO
	56.52	1.6269	13	0.334	(110) ZnO

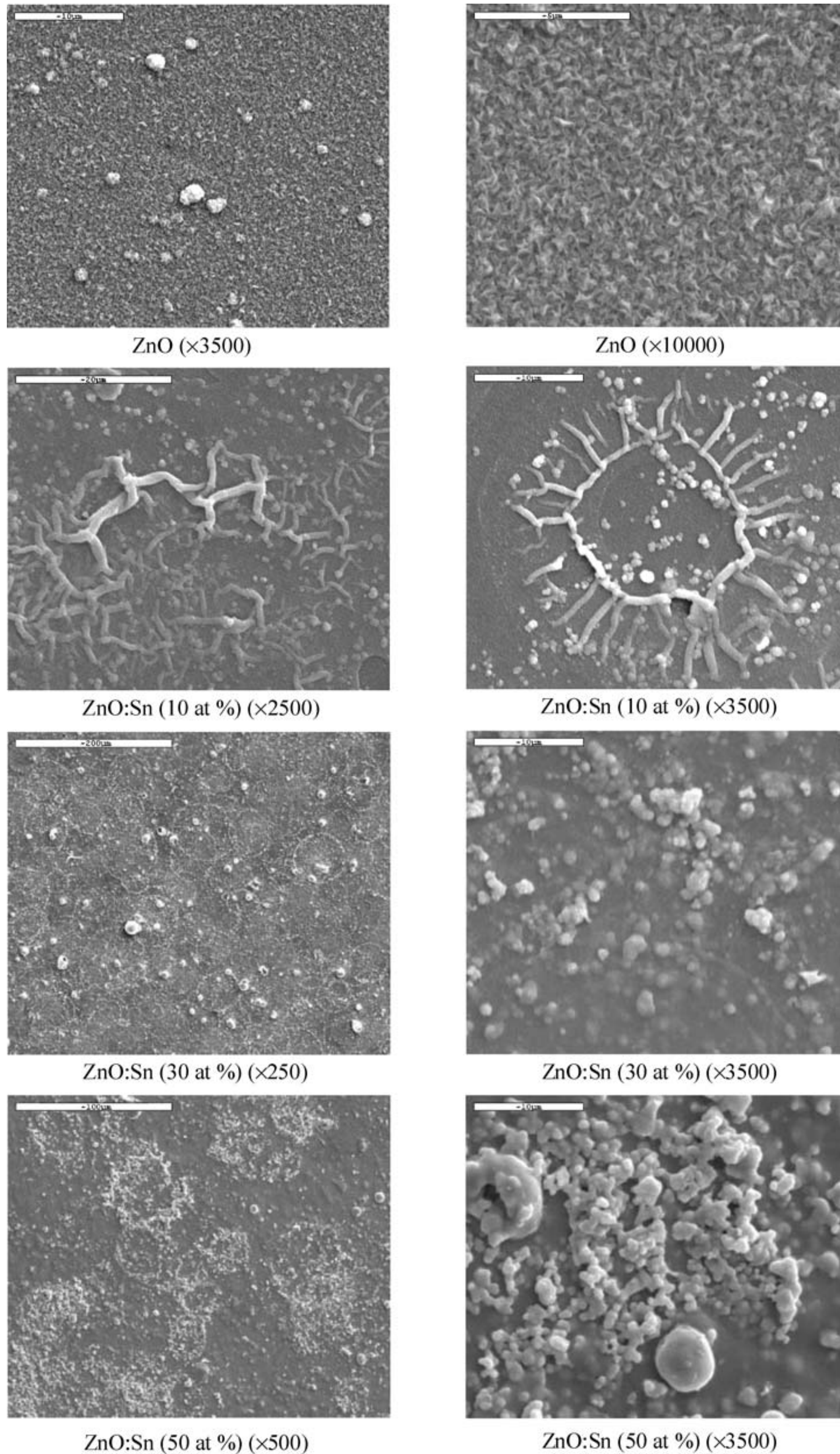

Figure 4 The SEM photographs of ZnO and ZnO:Sn films.

grains have *c*-axis perpendicular to the substrate surface. As the concentration of Sn in the precursor solution increased, the crystallinity is affected and the preferred orientation of ZnO films changes. ZnO:Sn films are composed of mixed crystallities of ZnO wurtzite, cubic Zn_2SnO_4 and tetragonal SnO_2 structures. The lattice spacing (d), angle of diffraction (2θ), relative intensity of the peaks (I/I_0) and the phases identified along with *(hkl)* planes of ZnO:Sn films are presented in Table IV. Both intensity and number of X-ray characteristic peaks for ZnO are significantly reduced when the concentration of Sn in the composition increased. The grain size in the films was estimated from the half-widths at the maximum of the X-ray diffraction for the peak with the highest intensity by using the classical Scherrer formula [28, 29], assuming that microstrain can be neglected. It vary from 10.4 to 41.6 nm (Table III). The preferential growth orientation of all

films was determined using the texture coefficient $TC(hkl)$. Using the expression [30–32]:

$$TC(hkl) = \frac{I(hkl)/I_0(hkl)}{N^{-1}\sum I(hkl)/I_0(hkl)}, \qquad (2)$$

where I is the measured intensity, I_0 is the ASTM standard intensity and N is the number of reflection. The preferential orientation of the film changes from (002) to (200) and (311) crystal plane with the increase of Sn concentration. As the Sn concentration of the precursor solution increases, Sn sits in the substitutional oxygen positions. In Fig. 3 the intensity of preferred orientation was decreased depending on the increasing Sn concentration. This decrease is mainly related to high concentration. The crystalline structure of the films deteriorates and tends to become amorphous which causes a reduction in the number of charge carriers and hence an increase in resistivity.

3.3. Surface morphologies

The surface morphologies of all films were investigated by SEM and are shown in Fig. 4. The surface morphologies of ZnO films are almost homogeneous. Depending on the increasing Sn concentration, the surface morphologies of the films were deteriorated. This result supports the XRD observations and show the transition of the material from crystalline to amorphous structure. These SEM micrographs show different morphologies of the surface grains, which depend on Sn concentration.

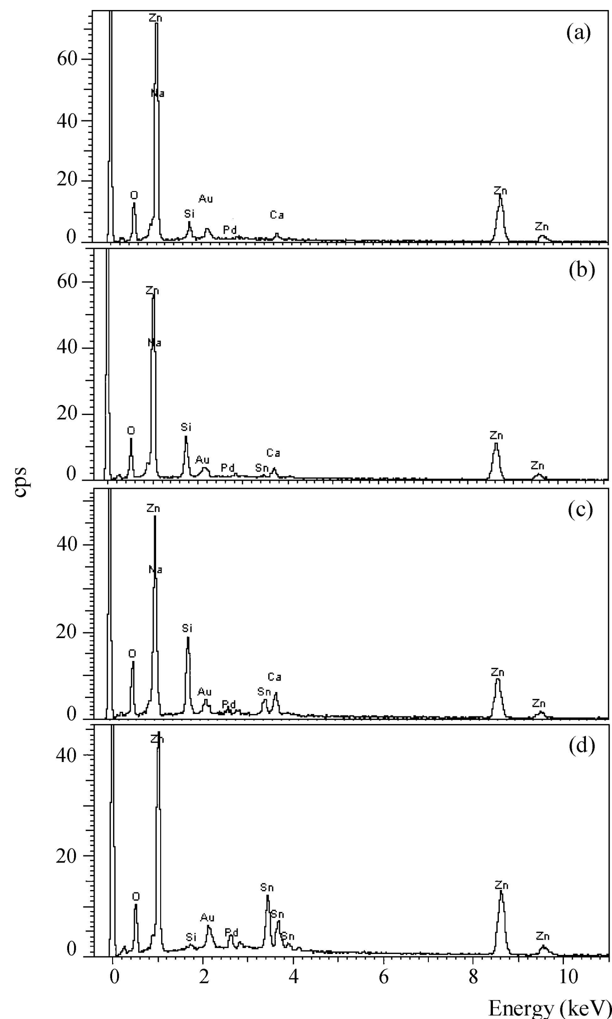

Figure 5 The EDS spectra of (a) ZnO, (b) ZnO:Sn (10at %), (c) ZnO:Sn (30at %), (d) ZnO:Sn (50at %) films.

TABLE V Elemental weight (at%) of Zn, Sn and O elements in the starting solution and solid film in respect to Sn concentration

	% El. weight in solution			% El. weight in solid film		
Material	Zn	Sn	O	Zn	Sn	O
ZnO	83.58	–	16.42	85.05	–	14.95
ZnO:Sn (10 at%)	75.02	8.61	16.37	84.65	0.26	15.09
ZnO:Sn (30 at%)	58.02	25.69	16.29	69.75	12.88	17.37
ZnO:Sn (50 at%)	41.22	42.59	16.19	62.42	21.57	16.01

3.4. EDS microanalyses

The elemental analyses of all films were investigated by EDS and are shown in Fig. 5. Zn, Sn and O elements are present in the film, and the amount of Zn decreases with increasing Sn concentration. The other elements (Si, Na and Ca) are not expected to be in the films and may have resulted from the glass substrates. Pd and Au elements resulted from the Au coating made before SEM studies. Elemental weights (at%) of Zn, Sn and O elements in the starting solutions and films in respect to Sn concentration are listed in Table V. The elemental weights in solution and solid film are not the same.

The optical absorbance and transmission spectra of ZnO and ZnO:Sn films were taken in the wavelength range 300–1100 nm using Perkin-Elmer Lambda 2S UV/VIS Double Beam spectrometer, but not presented here. The optical band gaps and average transmission values in the visible range of all films were found between 3.33–3.41 eV and about 40–80%, respectively. The band gap of ZnO films was increased and transmission of ZnO films was decreased with increasing Sn concentration in the precursor solution. To determine whether the films have direct or indirect band gap, plots of $(\alpha h\nu)^2$ versus $h\nu$ and $(\alpha h\nu)^{1/2}$ versus $h\nu$ were drawn. Better linearity was observed in the former case and it was determined that all films have a direct band transition. More details about optical properties of ZnO and ZnO:Sn films is given elsewhere [20].

4. Conclusion

ZnO and ZnO:Sn films, at the Sn percentages of 10, 30 and 50, prepared by USP technique and the effect of the Sn concentration on the electrical, structural and morphological properties of the ZnO films was investigated. First of all, we presented the results of DC conductivities of polycrystalline ZnO and ZnO:Sn films depending on the applied voltage and the temperature in dark conditions. It was seen that the resistivity of ZnO films decreases for lower Sn concentration (at 10%) and then increases for higher Sn concentration (at

30–50%). It was determined from the $I - V$ plots that ZnO and ZnO:Sn (at 50%) films have deep trapped structures, ZnO:Sn (at 10%) films have ohmic structure and ZnO:Sn (at 30%) films have shallow trapped structure. From the conductivity-temperature measurements, the overall temperature range for all the films can be divided into two regions as low and high temperatures. For these two regions, activation and donor-like trap energies (E_a and E_t) of all films were calculated. Depending on the increasing Sn concentration, E_t values of ZnO films decreased and E_a values of ZnO films increased. The XRD patterns showed that the as-deposited films have polycrystalline structure. The crystalline nature of the films was deteriorated with increasing Sn concentration and a shift to amorphous structure was seen. Besides, the preferential orientation of ZnO films also changed, the half peak widths increased and grain sizes decreased depending on the increasing Sn concentration. The effect of Sn concentration was to increase the surface roughening and change considerably the morphologies of ZnO films. The most homogenous surface was seen in ZnO films. These results are in good agreement with XRD observations. EDS results showed that all elements in the starting solutions were in the solid films and Zn element is more dominant than Sn on the surfaces. Consequently, we can say that ZnO and ZnO:Sn (at 10%) films may used as antireflecting coating and window material in solar cells due to their low resistivity and higher transparency in the visible range. The other films may be used in gas sensors where high conductivity is unnecessary.

Acknowledgements
This work was supported by Osmangazi University Research Fund under the Project Number of 2001/11.

References
1. M. ORTEGA, G. SANTANA and A. MORALES-ACEVEDO, *Superficies y Vacio* **9**, 294.
2. W. T. SEEBER, M. O. ABOU-HELAL, S. BARTH, D. BEIL, T. HÖCHE, H. H. AFIFY and S. E. DEMIAN, *Materi. Sci. Semicond. Process.* **2** (1999) 45.
3. P. NUNES, E. FORTUNATO and R. MARTINS, *Thin solid Films* **383** (2001) 277.
4. B. JOSEPH, K. G. GOPCHANDRAN, P. V. THOMAS, P. KOSHY and V. K. VAIDYAN, *Mater. Chem. Phys.* **58** (1999) 71.
5. F. PARAGUAY D., W. ESTRADA L., D. R. ACOSTA N., E. ANDRADE and M. MIKI-YOSHIDA, *Thin Solid Films* **350** (1999) 192.
6. F. M. AMANULLAH, K. J. PRATAP and V. HARI BABU, *Mater. Sci. Engng. B* **52** (1998) 93.
7. G. K. BHAUMIK, A. K. NATH and S. BASU, *ibid.* **52** (1998) 25.
8. K. B. SUNDARAM and A. KHAN, *Thin Solid Films* **295** (1997) 87.
9. YUNG-JEN LIN and CHING-JIUNN WU, *Surf. Coat. Techn.* **88** (1996) 239.
10. B. J. LOKHANDE and M. D. UPLANE, *Appl. Surf. Sci.* **167** (2000) 243.
11. D. R. ACOSTA, E. P. ZIRONI, E. MONTOYA and W. ESTRADA, *Thin Solid Films* **288** (1996) 1.
12. T. SCHULER and M. A. AEGERTER, *ibid.* **351** (1999) 125.
13. K. T. RAMAKRISHNA REDDY, H. GOPALASWAMY, P. J. REDDY and R. W. MILES, *J. Cryst. Growth* **210** (2000) 516.
14. S. SHANTHI, C. SUBRAMANIAN and P. RAMASAMY, *Mater. Sci. Engng. B* **57** (1999) 127.
15. B. Thangaraju, *Thin Solid Films* **402** (2002) 71.
16. A. K. IVANOV-SCHITZ, A. V. NISTUK and N. G. CHABAN, *Solid State Ion.* **139** (2001) 153.
17. I. TANIGUCHI, D. SONG and M. WAKIHARA, *J. Power Sourc.* **109** (2002) 333.
18. F. ATAY, S. KOSE, V. BILGIN and I. AKYUZ, *Mater. Lett.* **57** (2003) 3461.
19. F. ATAY, S. KOSE, V. BILGIN and I. AKYUZ, *Balkan Phys. Lett.* **10**(2) (2002) 70.
20. V. BILGIN, PhD Thesis, Osmangazi University, Turkey, 2003, p. 165.
21. F. ATAY, V. BILGIN, I. AKYUZ and S. KOSE, *Mater. Sci. Semicond. Process.* **6** (2003) 197.
22. M. A. LAMPERT and P. MARK, "Current Injection in Solids." (Academic Press, USA, 1970) p. 347.
23. K. C. KAO and W. HWANG, "Electrical Transport in Solids, International Series in the Science of the Solid State" (Pergamon Press, 1979) p. 663.
24. J. MA, F. JI, H. L. MA and S. Y. LI, *Solar Energy Materials Solar Cells,* **60** (2000) 341.
25. Y. IGASAKI and H. KANMA, *Appl. Surf. Sci.* **169**/170 (2001) 508.
26. H. KIM, A. PIQUE, J. S. HORWITZ, H. MURATA, Z. H. KAFAFI, C. M. GILMORE and D. B. CHRISEY, *Thin Solid Films* **377–378** (2000) 798.
27. T. K. SUBRAMANYAM, B. SRINIVASULU NAIDU and S. UTHANNA, *Optical Mater.* **13** (1999) 239.
28. A. S. RIAD, S. A. MAHMOUD and A. A. IBRAHIM, *Physica. B* **296** (2001) 319.
29. B. D. CULLITY, "The Elements of X-Ray Diffraction" 2nd ed. (Addison-Wesley, Reading, MA, 1978).
30. C. BARRETTA and T. B. MASSALASKI, "Structure of Metals" (McGraw-Hill, New York, 1966) p. 205.
31. S. A. NASSER, H. H. AFIFY, S. A. EL-HAKIM and M. K. ZAYED, *Thin Solid Films* **315** (1998) 327.
32. H. H. HUANG and M. H. HON, *J. Cryst. Growth* **222** (2001) 540.

Received 4 October
and accepted 7 October 2004